1   # POU4F2/BRN3B OVEREXPRESSION PROMOTES THE GENESIS OF RETINAL GANGLION CELL-LIKE
2   PROJECTION NEURONS FROM LATE PROGENITORS

3

4   **Authors:** Oliveira-Valença, V.M.[1]; Roberts, J.M[3]; Fernandes-Cerqueira, V.M. [1]; Colmerauer, C.H. [1];
5   Toledo, B.C.[1]; Santos-França, P.L.[1, #]; Linden, R.[1]; Martins, R.A.P.[2]; Rocha-Martins, M[1,&]; Bosco, A.[3];
6   Vetter, M.L.[3]; Silveira, M.S.[1]
7   [1]Instituto de Biofísica Carlos Chagas Filho, Universidade Federal do Rio de Janeiro, Av. Carlos Chagas Filho 373,
8   21941-902 Rio de Janeiro, Brazil
9   [2]Instituto de Ciências Biomédicas, Universidade Federal do Rio de Janeiro, Av. Carlos Chagas Filho 373, 21941-
10   902 Rio de Janeiro, Brazil
11   [3] Department of Neurobiology, University of Utah, School of Medicine, Salt Lake City, UT 84112, USA.
12   [#] current address: Cellular Neurobiology Research Unit, Institut de recherches cliniques de Montréal (IRCM),
13   Montreal H2W 1R7, Canada
14   [&]current address: Max Planck Institute for Molecular Biomedicine Röntgenstraße 20, 48149, Münster, Germany

15

16   ## ABSTRACT

17   Retinal ganglion cells (RGCs) are the projection neurons of the retina. In early retinal progenitor cells
18   (RPCs), *Atoh7* orchestrates the developmental RGC program and regulates the expression of critical
19   downstream targets, including *Pou4f* factors. The absence of *Pou4f2* or more POU4F family genes
20   results in defects in RGC differentiation, aberrant axonal elaboration and ultimately RGC death,
21   confirming the requirement of POU4F factors for RGC development and survival, with a critical role
22   in regulating RGC axon outgrowth and pathfinding. Here, we investigated *in vivo* whether ectopic
23   *Pou4f2* expression in late retinal progenitor cells (late RPCs) is sufficient to induce the generation of
24   cells with RGC properties, including projecting axons to the brain. Using a strong ubiquitous promoter
25   to induce *Pou4f2* overexpression in neonates, we observed a change in targeted cell distribution in
26   the retinal tissue, including the presence of cells in the ganglion cell layer and inner plexiform layer
27   with high density of GFP$^+$ processes along the retina. Similar results on the induction of neuron
28   processes were obtained when we overexpressed *Pou4f2* in *Atoh7* knockout mice, suggesting that
29   POU4F2 is sufficient to induce them. Single-cell RNA sequencing (scRNA-seq) analysis shows that
30   several RGC-genes (such as *Rbpms*, *Gap-43*, *Hs6st3*, and *Foxp2*) are upregulated after *Pou4f2*
31   overexpression. Additionally, gene ontology analysis indicates the induction of genes related to
32   axonogenesis and neuronal differentiation. Imaging throughout the visual pathway revealed high
33   density of axons projecting toward the optic nerve head and extending to brain regions, such as the
34   superior colliculus and geniculate nucleus. Thus, *Pou4f2* induced neurons with specific RGC
35   characteristics that share similarities with resident RGCs and notably project axons that reach brain
36   targets. In conclusion, these results showed that POU4F2 alone was sufficient to promote critical
37   properties of projection neurons from retinal progenitors outside their developmental window.

38

39

40

41   **Keywords:** *Pou4f2/Brn3b*; late progenitors; axonogenesis; RGC-like cells

42

43   INTRODUCTION

44   Retinal ganglion cells (RGCs) constitute a unique cell population of the retina capable of
45   extending long axons that reach specific brain regions and establish connections. At least 40 subtypes
46   of RGCs have been described based on their transcriptional profile and functions (Rheaume et al.,
47   2018). The ability to project long distance axons is one of the most critical characteristics of RGCs that
48   must be attained in regenerative strategies aimed at restoring vision. Several neuropathies lead to
49   RGC death, such as glaucoma, optic nerve traumas and diabetic retinopathy (Fechtner & Weinreb,
50   1994; Quigley, 1995; 1999; Halpern & Grosskreutz, 2002; Gupta & Yucel, 2007; Danesh-Meyer &
51   Levin, 2015; Gossman et al., 2016; Killer & Pircher, 2018). RGC degeneration in glaucoma alone is
52   expected to blind 111.8 million people worldwide in 2040 (Tham et al., 2014).

53   To mitigate the damage from these neuropathies, current research seeks to either decelerate
54   cell loss through RGC neuroprotection or to restore vision via the generation of new RGCs. The
55   potential regenerative cell sources are either manipulated endogenous retinal cells or exogenously
56   generated from embryonic or induced pluripotent stem cells (Gossman et al., 2016; Tanaka et al.,
57   2016; Chao et al., 2017; Oliveira-Valenca et al., 2020; Luo & Chang, 2023; Sharma et al., 2023; Soucy
58   et al., 2023; Tribble et al., 2023). Müller glia (MG), the main endogenous cell source currently under
59   investigation, share epigenetic and transcriptional profiles with the late retinal progenitor cells (late
60   RPCs) (Blackshaw et al., 2004; Ooto et al., 2004; Roesch et al., 2008; Dvoriantchikova et al., 2019).

61   During retinal development in rodents, late RPCs give rise to most rod photoreceptors (RPs),
62   and also to bipolar cells (BCs), subpopulations of amacrine cells (ACs), and MG in the postnatal period.
63   On the other hand, early RPCs generate RGCs, horizontal cells (HCs), some ACs and cone
64   photoreceptors (CPs) during the embryonic period (Finlay et al., 1989; Saha et al., 1992; Hu et al.,
65   1999; Chow et al., 2001; Bassett & Wallace, 2012; Clark et al., 2019).

66   Specific molecular programs are activated and restricted to establish the competence of
67   retinal progenitors (RPCs) to differentiate into distinct cell populations and build the mature,
68   functional retina (Young, 1985; Rapaport et al., 2004; Heavner & Pevny, 2012; Centanin & Wittbrodt,
69   2014; Zechner et al., 2020). Thus, any strategy designed to regenerate functional RGCs will have to
70   reactivate key steps of this gene regulatory network (GRN).

71   *Atoh7* is an essential competence factor that induces the RGC molecular program (Yang et
72   al., 2003; Mu et al., 2005; Le et al., 2006; Yao et al., 2007; Gao et al., 2014; Maurer et al., 2018; Wu
73   et al., 2021). Crucial downstream effectors of *Atoh7* in the RGC gene regulatory network are the POU
74   domain, class 4, transcription factors (POU4F1-3) (Liu et al., 2001; Mu et al., 2005). Several studies
75   have demonstrated that the absence of POU4F2 compromises axonogenesis, as RGCs exhibit
76   aberrant projection along the retina and a thinner or absent optic nerve. Additionally, knockout
77   experiments have shown that even when some RGCs differentiate, they eventually die due to failure
78   to stabilize connections to the brain, thereby demonstrating the role of *Pou4f2* in axonogenesis and
79   survival (Erkman et al., 1996; Gan et al., 1996; Xiang et al., 1996; Gan et al., 1999; Erkman et al.,
80   2000). Some studies also suggest that *Pou4f2* could have a role in RGC specification by suppressing
81   genes required for alternative cell fates including amacrine cells and cones (Qiu et al., 2008; Feng et
82   al., 2011). Shi et al. (2013) demonstrated that besides repressing some cell fates, *Pou4f2* is important
83   to induce the generation of POU4F1[+]/3[+] and melanopsin RGC subtypes. Moreover, Rasheed et al.
84   (2014) show that *Pou4f2* is expressed in two distinct waves regulated by miRNAs during retinal

85　development and theorize that in early stages it would play a role in RGC specification and, later, in
86　survival and axon guidance.

87　POU4F2 does not solely work with POU4F members but can also act in conjunction with ISL1
88　to promote RGC differentiation (Pan et al., 2008; Li et al., 2014; Wu et al., 2015), as well as with
89　DLX1/2 (de Melo et al., 2005; Zhang et al., 2017) and EOMES for RGC development and formation of
90　the optic nerve (Mao et al., 2008). Liu et al. (2000) tested the overexpression of *Pou4f2* during the
91　window of RGC generation in chick (thus in the presence of *Atoh7*) and observed an increase in RGC
92　genesis, suggestive of the sufficiency of this factor to induce RGCs. Moreover, Wu et al. (2015)
93　showed that the combination of POU4F2 with ISL1 was enough to induce RGC specification even in
94　the absence of *Atoh7*, demonstrating that this factor could also play a role for RGC specification when
95　combined with other factors. Interestingly, Todd et al. (2022) demonstrated the *in vivo* conversion of
96　murine Müller glia into RGC-like cells after the combined overexpression of *Ascl1*, *Pou4f2* and *Isl1*.
97　These neurons acquired an immature RGC transcription profile, similar to RGCs in the beginning of
98　their specification, however they did not observe axons in the optic nerve.

99　Given that *Pou4f2* plays essential roles in RGC development and axonogenesis, our goal in
100　this study was to test whether its overexpression as a single transcription factor in late RPCs could
101　reactivate aspects of the RGC molecular program relevant for RGC differentiation, especially axon
102　growth and pathfinding, outside of their development window. We show that *Pou4f2* overexpression
103　indeed induces the generation of RGC-like cells from late RPCs, which migrate to the inner retina and
104　project axons toward the optic nerve head, along the entire visual pathway and to multiple brain
105　targets. Single cell RNA sequencing (scRNA-seq) reveals the generation of cells expressing RGC genes
106　upon *Pou4f2* overexpression, including genes involved in axonogenesis.

107　Overall, these data demonstrate that overexpression of *Pou4f2* is sufficient to induce the
108　expression of several RGC features in late progenitors, remarkably axonogenesis, as projections
109　innervate appropriate central visual targets in adult mice.

110 **MATERIALS AND METHODS**

111 *Experimental animals*

112 All experiments were performed according to international rules and were approved by the Ethics

113 Committee on Animal Experimentation of the Health Sciences Center from Federal University of Rio

114 de Janeiro (CEUA/CCS/UFRJ) and within the guidelines of the Institutional Animal Care and Use

115 Committee of the University of Utah. Both sexes of neonatal (P0, postnatal day 0) Lister hooded rats

116 (RRID:RGC 2312466), C57Bl6/J mice (RRID:IMSR_JAX:000664) and B6J.129-Atoh7$^{tm1Gla/Mmucd}$

117 (MGI2159015, mentioned here as Atoh7KO), were used for *in vivo* electroporation and analyzed 10

118 or 30 days post electroporation.

119

120 *Plasmids*

121 Plasmids pUb::CST (pUb- human ubiquitin C promoter) and pUb::GFP (Matsuda & Cepko, 2004) were

122 kindly provided by Dr. Michael A. Dyer (St. Jude Hospital, Tennessee, USA). POU4F2 sequence was

123 obtained from CMV::Brn3b plasmid (CAT#:MR223071, Origene) using the restriction enzymes NotI

124 and EcoRI. This fragment was inserted into pUb::GFP vector (previously digested with NotI and Age1)

125 to generate the pUb::Pou4f2 using the oligonucleotide sequences: 5'-

126 GGCCGCTGTAAGCCGTAACGACTAACTCTGC – 3' and 5' - CGACATTCGGCATTGCTGATTGAGACGAGCT -

127 3' to introduce appropriate cut sites. The final concentration of plasmid solution was 5 µg/µL either

128 for control (pUb::CST 70% pUb::GFP 30%) or POU4F2 (pUb::Pou4f2 70% pUb::GFP 30%) experimental

129 groups.

130

131 *In vivo electroporation and EdU incorporation*

132 This procedure was performed as described previously (Matsuda & Cepko, 2007; Rocha-Martins et

133 al., 2019). Briefly, P0 Lister hooded rats or mice were anesthetized by hypothermia and the plasmid

134 solution was injected into the subretinal space with a Hamilton syringe with 33G blunt end needle (1

135 µL or 0.5 µL, respectively to rats or mice, of a 5.0 µg/µL solution containing 0.1% Fast Green Dye (cat#

136 14335, Cayman Chemical)). Five 99V pulses were applied for 50 ms with 950 ms intervals using a

137 forceps-type electrode (Nepagene, CUY650P7) with Neurgel (Spes Medica). After temperature

138 recovery, pups were returned to the original cage. To avoid variability, both control and experimental

139 groups were from the same litter. Pups received EdU by subcutaneous injection (10µl 2.5mM

140 EdU/gram of body weight, Invitrogen #C10637) at P0 and P1 after the electroporation procedure.

141

142 *Immunofluorescence*

143 Protocols used were described previously (Rocha-Martins et al., 2019). Eyes were fixed by immersion

144 in 4% paraformaldehyde in phosphate buffered saline (PBS) overnight, cryoprotected in 30% sucrose

145 in PB, and then immersed in OCT for the preparation of transversal cryosections (10µm) that were

146 mounted on microscope slides treated with 6% silane (cat#440140, Sigma). Electroporated retinas,

147 optic nerves (14µm) and brain cryosections (35µm) were immunoreacted with different primary

148 antibodies (RBPMS, #1830-RBPMS/Phosphosolution, Lot#NB1117g; CHX10, X1180P/Exalpha,

149 Lot#13877; SOX9, AB5535/Milipore, Lot#3063352; NEUN/RBFOX3/Milipore, MAB377, Lot#2453249;

150 RHO, ab98887/Abcam; GAP-43, sc-1086/Santa Cruz) combined with anti-GFP (mAB3E6/Invitrogen

151 Lot#2094035 or A11122/ Invitrogen Lot# 2273763). For the analyses of wholemount retinas, the eyes

152　were fixed overnight in 4% paraformaldehyde and retinas dissected and immersed in 0.5% Triton X-
153　100 for at least 30 minutes. The retinas were then incubated in blocking solution (5% horse serum in
154　2% Triton X-100) for 1 hour and incubated with primary antibodies for at least 2 days, with slow
155　shaking at 4°C. EdU labelling was performed following the guidelines of the kit (Click-iT™ EdU Cell
156　Proliferation Kit for Imaging, Alexa Fluor™ 647 dye, C10340, Invitrogen).

157

158　*Image acquisition*
159　For transverse sections from rat retinas immunostained with antibodies for GFP and specific cell
160　markers, images were acquired using a structural illumination microscope (Imager M2, ApoTome,
161　Zeiss) with Plan-Apochromat 20x/0.8 objective and AxioCam MRm camera. EdU and GAP43 labelling,
162　as well as mouse brains were imaged using a 20x/0.8 by confocal microscopy (Nikon A1, Eclipse Ti2).
163　Wholemount retinas were imaged using oil 40x/1.15 objective by confocal microscopy (Leica TCS-SPE
164　with an AOBS system). Image acquisition settings were maintained across replicate experiments.
165　Software used for image acquisition were Zen Blue, LasX and NIS-Elements. Image processing
166　included the use of maximum intensity projection (MIP) tool and color change and adjustments in
167　brightness in Image J/Fiji. GAP-43 insets (**Figure 2E**) represent one slice of 0.8 µm thickness and the
168　main image was generated using the MIP tool. In the wholemount analysis from Atoh7KO mice
169　(**Figure 3**), we defined the layers using the DAPI staining (and looking at the distance between two
170　nuclei) followed by MIP processing. Images were cut and rotated in Adobe illustrator, which was also
171　used for the manual reconstruction of the optic nerve and optic chiasm from images acquired by
172　structured illumination microscopy.

173

174　*Quantitative and statistical analyses*
175　Representative images from retinal cryosections were selected for quantitative analyses. In
176　electroporated retinas, 200 to 500 GFP$^+$ cells were counted in all the three nuclear layers for each
177　animal analyzed using Zen Blue software or ImageJ 1.54f. The results were plotted as mean ± SEM
178　with adjusted p value. The statistical analyses were performed using Two-way ANOVA with multiple
179　comparisons and corrected using Sidak's test (graphs from **Figure 1C**, **E** and **Figure S1 D**). For the
180　graph in **Figure 1G**, unpaired t-test (two-tailed p value) was performed. Alpha value used was 5.0%.
181　For all analyses, GraphPad Prism software version 8.0.2 was used.

182

183　*scRNA-seq sample preparation*
184　Wild type mice at P0 or P1 were electroporated with the plasmid preparations Pou4f2-GFP or GFP
185　alone injected into the subretinal space. Ten days later, retinas were collected for dissociation.
186　Electroporated retinas were dissociated using papain as described before in Justin Brodie-Kommit et
187　al. (2021). Briefly, papain solution (100 µL papain – 10mg/mL – containing 110 µL of 50mM L-cysteine,
188　110 µL of 10mM EDTA, 10 µL of 60mM 2-Mercaptoethanol) was pre-incubated at 37°C for 30 minutes
189　before the dissociation. After that, two retinas were added to the papain solution and incubated for
190　10 minutes at 37°C. 50 µL of DNAse (1mg/mL) was added after 5 minutes of dissociation. To block
191　the reaction, 2.5 mL of neurobasal supplemented with 10% FBS and 500 µL of ovomucoid (10mg/mL)
192　were added. Tubes were spun down for 5min, 300RCF at 4°C and resuspended in 500 µL of
193　neurobasal+10% FBS. Single, viable, GFP$^+$ cells were isolated by cell sorting with BD FACSAria 4 laser

194   instrument using 70μm nozzle size and collected into 20 μL DMEM + 5% FBS. Multiple retinas were

195   combined as necessary to obtain 30k GFP$^+$ cells for each condition.

196

197   *scRNA-seq Library prep and Sequencing*

198   Library generation and sequencing were performed by the Huntsman Cancer Institute High-

199   Throughput Genomics and Bioinformatics Analysis Shared Resource. Sorted cells were prepared with

200   the 10X Genomics Next GEM Single Cell 3' Gene Expression Library prep v3.1 with UDI. The library

201   was chemically denatured and applied to an Illumina NovaSeq flow cell using the NovaSeq 150x150

202   bp XP workflow (20043131). Following transfer of the flow cell to an Illumina NovaSeq 6000

203   instrument, a 150 x 150 cycle paired end sequence run was performed using a NovaSeq 6000 S4

204   reagent Kit v1.5 (20028312). Sequencing was performed to a depth of at least 200M paired

205   reads/sample.

206

207   *scRNA-seq Analysis*

208   Fastq files were aligned to the mouse transcriptome index for mm10 and GFP using cellranger-7.0.1

209   with expected cells set to 5000. The final number of cells for each condition were: 7,722 control and

210   9,187 *Pou4f2* overexpression (Pou4f2 OE). The filtered matrix output from cellranger was imported

211   to Seurat v4.3.0.1 and further filtered for cells with less than 4% mitochondrial transcripts, more than

212   1,200 genes, and fewer than 25,000 transcripts. The control and Pou4f2OE (OE- overexpression)

213   datasets were merged, and SCTransform v0.3.5 pipeline run with all default settings. Clusters were

214   annotated with known markers for retinal cells and combined as appropriate based on those markers

215   (**Table S1** and **Figure 2**). Cluster markers and differentially expressed genes between the experimental

216   conditions were defined using the FindAllMarkers and FindMarkers functions respectively, using

217   default settings (**Tables S4** and **S5**). Integration with developmental data was achieved using Clark et

218   al. Specifically, the developmental dataset was subset for only those cells used for pseudotime

219   analysis, as defined in the cell metadata, and merged with the Pou4f2 single cell dataset. These were

220   combined with the Seurat v5.1.0 IntegrateLayers function using CCA integration (**Figure 4**).

221

222   *Gene Set Enrichment Analysis*

223   Gene set enrichment analysis was run on the scRNA-seq Pou4f2 OE dataset using gene sets obtained

224   from the Molecular Signatures Database. Specifically, we used the mouse-M5 ontology gene sets

225   v2023.2. All detectable genes were ranked by average log2 fold change between all control and

226   Pou4f2 OE cells and analyzed with fgsea v1.27.0 using default settings. The results from this analysis

227   are in **Table S3** and **Figure 5**.

228

229

230

RESULTS AND DISCUSSION

Overexpression of *Pou4f2* impacts the fate of late RPCs

The loss of POU4F2 impacts RGC terminal differentiation and survival, through its significant role in axon growth and pathfinding (Erkman et al., 1996; Gan et al., 1996; Xiang et al., 1996; Gan et al., 1999; Erkman et al., 2000). To investigate whether overexpression of *Pou4f2* in late RPCs can promote aspects of RGC differentiation, we performed subretinal *in vivo* electroporation at postnatal day 0 (P0) (Matsuda & Cepko, 2004). (**Figure 1A**). The mature retina is a stratified tissue composed of three nuclear layers where specific cell types are precisely arranged (Dowling, 1987; Livesey & Cepko, 2001; Amini et al., 2017). In line with the known competence of late RPCs, analysis of control retinas 10 days after electroporation showed that the majority of GFP$^+$ cells were in the outer nuclear layer (ONL) (81.58 ± 3.76%), fewer were in the inner nuclear layer (INL) (18.56 ± 3.71%), and none to the ganglion cell layer (GCL) (**Figure 1B and 1C**). In comparison, retinas co-electroporated with plasmids for *Pou4f2* and GFP showed fewer GFP$^+$ cells at the ONL (67.25 ± 3.04%), a subtle increase in the INL (28.82 ± 3.14%, p=0.0484) and some GFP$^+$ cells localized to the ganglion cell layer/inner plexiform layer (GCL-IPL) (3.93 ± 0.47%) (**Figure 1B and C**). These data suggest two major possibilities: i) *Pou4f2* promotes a change in the cell fate of late RPCs, or ii) *Pou4f2* affects the migration of cells derived from late RPCs.

To test the first hypothesis, we performed immunostaining to characterize the identity of GFP$^+$ cells. Examining retinas 30 days after *Pou4f2* co-electroporation, we identified GFP$^+$ cells which were RBPMS$^+$ (a specific RGC marker) in wholemount retinas, while this was not observed after GFP electroporation alone. These RBPMS$^+$GFP$^+$ cells were in the GCL (left panel) and in the INL (right panel) with some exhibiting complex branching (**Figure 1D**). Quantification 10 days after *Pou4f2* electroporation revealed a significant increase in the proportions of RBPMS$^+$ and NEUN$^+$ (expressed by both amacrine cells and RGCs) among the GFP$^+$ cells relative to controls (**Figure 1E**).

Besides RGC markers, we also immunostained against specific markers for late-born cell types such as rod photoreceptors (RHO$^+$), bipolar cells (CHX10$^+$) and Müller glia (SOX9$^+$), to evaluate whether *Pou4f2* overexpression changes the fate of a specific cell population (**Figure S 1 A-D**). *Pou4f2* significantly reduced the number of RHO$^+$GFP$^+$ cells whereas no significant changes were found in the numbers of bipolar cells (CHX10$^+$) or Müller glia (SOX9$^+$) (**Figure S 1 D**). These data suggest that the change in gene expression occurs mostly in progenitors that would normally generate rod photoreceptors.

To confirm whether these cells were derived from late retinal progenitors we performed lineage-tracing experiments through EdU incorporation in cycling cells. EdU was injected at P0 and P1 (followed by electroporation in P1) to label some late RPCs and their daughter cells (**Figure 1A**). Previously, we established that this experimental design resulted in EdU labeling of more than half of GFP$^+$ late RPCs and their progeny (62.55 ± 1.97%) after 10 days. Around 16.44 ± 2.70% of this population (GFP$^+$EdU$^+$) were RBPMS$^+$ cells (**Figure 1F and G**) showing that they are newborn cells generated upon *Pou4f2* overexpression. Together, these changes in both gene expression and laminar localization support that *Pou4f2* overexpression induces a cell fate change in late RPC-derived cells.

273 **Transcriptome analysis reveals induction of RGC and axonogenesis genes**

274   To further characterize the gene expression profile of the *Pou4f2*-induced cells, we isolated

275 GFP-labeled cells by FACS after electroporation with plasmids for GFP alone (CTR) or together with

276 *Pou4f2*, then performed single cell RNA-sequencing (scRNA-seq). Uniform manifold approximation

277 and projection (UMAP) analysis enabled the identification of cells that share transcriptional profiles

278 and can be classified as specific cell types (Becht et al., 2019). Using previously reported cell type

279 specific markers (**Table S1**) (Macosko et al., 2015), we were able to define clusters of late-born cell

280 types among GFP⁺ cells. Similar to the results of our immunostaining experiments (**Figure S1 D**), the

281 majority of control cells were identified as rod photoreceptors (67.2%), a smaller portion as bipolar

282 cells (19.4%), and the minority as Müller glia (6.6%), amacrine cells (4.4%) or cones (1.7%) (**Figure 2B**

283 **and Figure S1 D and E**). In addition, clusters unique to the *Pou4f2* OE sample were identified (**Figure**

284 **2A**, blue dots), indicated as clusters 1, 2, 3 and 4 (**Figure 2B** and **C**). In these *Pou4f2*-clusters (1-4), we

285 detected enrichment of RGC-specific genes, such as *Rbpms* (HÖRNBERG et al., 2013; Rodriguez et al.,

286 2014), *Hs6st3 (Conway et al., 2011)*, *Foxp2* (Rousso et al., 2016; Sato et al., 2017) and *Gap43* (Reh et

287 al., 1987; Kruger et al., 1998) (**Figure 2D**). Moreover, immunostaining for GAP-43 validated scRNA-

288 seq data, showing GAP-43⁺GFP⁺ cells after *Pou4f2* overexpression, but not in control condition (**Figure**

289 **2E**). Again, consistent with our immunostaining the proportions of rod photoreceptors (34.2%) are

290 reduced in favor of novel POU4F2 cell clusters 1-4 (29.4%). There was a reduction in the proportion

291 of bipolar cells (15.5%) and an increase in Müller glia (16.6%) with the caveat that Müller glia and

292 cluster 2 share similarities at the transcriptional level (**Figure S1 E**). This data reinforces that *Pou4f2*

293 overexpression is sufficient to induce changes in the fate of late RPCs, allowing the generation of

294 RGC-like cells from a subset of these progenitors.

295   Since the role of POU4F2 on RGC specification is incompletely understood (Gan et al., 1996;

296 Xiang, 1998; Rasheed et al., 2014), we hypothesize that several mechanisms may be linked to the

297 genesis of RGC-like cells upon *Pou4f2* overexpression (**Figure 1D** and **Figure 2D**). *Pou4f2* may

298 reprogram a subset of late RPCs through an *Atoh7*-independent pathway (Justin Brodie-Kommit et

299 al., 2021) or induce RGC-related genes in a subset of ATOH7⁺ late RPCs. Indeed, Miesfeld et al. (2018)

300 identified ATOH7⁺ cells in the proliferative layer of the mouse retina at P0. Alternatively, *Pou4f2* may

301 induce RGC characteristics in cells generated from late RPCs through the direct induction of a partial

302 repertoire of RGC genes, such as those responsible for axonogenesis.

303   To explore these hypotheses, we overexpressed *Pou4f2* in *Atoh7* knockout mice (Atoh7KO)

304 and tested whether the generation of RGC-like cells and projections occur. We first analyzed the cell

305 distribution of GFP⁺ among retinal layers and we found cells located at the ganglion cell layer when

306 *Pou4f2* was overexpressed (**Figure 3A inset 6, B and D**), which is not detected in the control condition

307 (we only detect GFP⁺ MG-end feet, (**Figure 3A inset 3**). When we performed the immunostaining for

308 RBPMS after *Pou4f2* overexpression, even though we could not clearly detect neither GFP⁺RBPMS⁺

309 nor GFP⁻RBPMS⁺ cells, we identified neurons with complex morphology and aberrant projections

310 which presented a random trajectory or even were directed to the periphery of the retina (**Figure 3A**

311 **insets 5, 6 and B**). GFP⁺ projections were disorganized probably as a consequence of the absence of

312 axons from the resident RGCs and, consequentially, the optic nerve. These data suggest that, even in

313 the absence of *Atoh7*, *Pou4f2* can induce RGC properties, such as to project axons.

314   To identify POU4F2-direct targets that could promote changes in the transcriptional profile,
315 we compared differentially expressed genes (DEGs) from our dataset with previously published
316 POU4F2 CUT&TAG data (Ge et al., 2023). Ge et al. identified 313 genes with one or more nearby
317 POU4F2 binding sites. When we compared these putative POU4F2 target genes to the 316
318 upregulated genes from our scRNA-seq dataset, we observed an intersection of 33 genes (**Figure 2F**),
319 indicating that POU4F2 could have directly induced the expression of these genes. UMAP visualization
320 of the overlapping 33 genes revealed that most of these direct POU4F2-targets were expressed
321 specifically in the new clusters exclusively generated after *Pou4f2* overexpression (**Figure S2** and
322 **Table S2**). Interestingly, many of the overlapping genes are regulators of axon growth, which is
323 consistent with previous studies (Gan et al., 1999; Erkman et al., 2000). These results show that
324 POU4F2 could directly induce changes in the transcriptional profile favoring axonogenesis.
325   Additionally, to test whether these RGC-like cells were transcriptionally similar to RGCs
326 generated during development, we integrated our scRNA-seq data with a previously published
327 dataset (Clark et al., 2019) encompassing all cell types during retinogenesis (E11-P14). This allowed
328 us to compare the new clusters generated upon *Pou4f2* overexpression with early-born cell types, as
329 well as early and late RPCs (**Figure 4A**). Interestingly, we saw those cells from clusters 3 and 4, as well
330 as some cells from clusters 1 and 2, were close to the RGC cluster in UMAP representation, suggesting
331 that these newly generated cells shared transcriptional similarities with RGCs at a certain level (**Figure
332 4A and B**).
333   To represent the distribution of cells from clusters 1-4 that share similarities with RGCs in
334 Clark et al., we recolored these cells as dark gray (**Figure 4C**) and plotted them back onto the first
335 UMAP generated with only our control (CTR) and POU4F2 datasets (**Figure 4D**). This analysis revealed
336 that RGC-like cells from cluster 1 and cluster 2 are positioned at the tip of these clusters, with some
337 cells from cluster 2 closer to cluster 3. The results suggest that *Pou4f2* overexpression was able to
338 induce an RGC-related fate in some cells from clusters 1-4, that are transcriptionally similar to RGCs
339 generated during development.
340   To define the biological processes induced by *Pou4f2* overexpression, we performed gene
341 ontology (GO) analysis on our scRNA-seq results. This analysis revealed upregulation of genes
342 involved in several neurogenic processes, including axon development, neurogenesis, and synapse
343 organization. Conversely, phototransduction and photoreceptor maintenance genes were
344 downregulated, which could be attributed to the reduction in the population of rod photoreceptors
345 (**Figure 5AB, Table S3**). Further, volcano plot analysis highlights specific genes from the above-
346 regulated biological processes, demonstrating upregulated genes related to axonogenesis (red dots)
347 and downregulated phototransduction genes (blue dots). Notably, RGC-specific markers (SNCG and
348 FOXP2) were significantly upregulated in Pou4f2 OE (**Figure 5B and Table S4**).
349   UMAP visualization of the gene expression pattern of selected genes linked to axon
350 development by GO analysis, such as *Olfm1* (Nakaya et al., 2008; Nakaya et al., 2012), *Tubb3*, *Dclk1*
351 (Nawabi et al., 2015) and *Tenm4* (Young et al., 2023), showed their elevated expression in the new
352 clusters (1-4) generated by *Pou4f2* overexpression (**Figure 5C**), including *GAP43* (**Figure 2D**).
353 Importantly, 12 of the 33 genes we've described as direct POU4F2-targets are in the axon
354 development GO category (Ge et al., 2023) (**Figure S2**).

355   We also found in our scRNA-seq data other genes that may play important roles in
356   axonogenesis (**Figure 2F** and **Table S2**). For example, *Nav2* (Neuron navigator 2) is responsible for
357   regulating normal cranial nerve development and neurite outgrowth (McNeill et al., 2010) and may
358   play an axonal outgrowth role in RGC-like cells. Additionally, *Ebf1*, Early B-Cell Factor 1, is important
359   for correct axonal topography in the optic chiasm (Jin & Xiang, 2011), in the same way as *Tenm4* (*Ten-*
360   *m/Odz/teneurin 4*) was described to play a role in binocular circuits, while its absence impacts
361   contralateral projections to specific targets (Young et al., 2023). These genes are upregulated in one
362   or more of the new clusters generated upon *Pou4f2* overexpression (**Figure S2** and **Table S5**). In
363   conclusion, these data show that *Pou4f2* induces genes which are critical for axon growth, and some
364   of them are described as direct targets of POU4F2.
365
366   ### *Pou4f2*-induced RGC-like cells project axons that reach the brain
367   To verify if the axonogenesis genes induced by *Pou4f2* would be sufficient for the RGC-like
368   cells to extend axons through the retina, we first analyzed the presence of GFP⁺ processes in retinal
369   transversal sections and wholemounts 10 or 30 days after electroporation, respectively. Images of
370   central retinal sections showed GFP⁺ projections extending to the optic nerve head (ONH) 10 days
371   after *Pou4f2* overexpression (**Figure 5D**). After 30 days, confocal images from retinal wholemounts
372   displayed high density of projections at the GCL+NFL, most of them organized and directed toward
373   the optic nerve head (**Figure 5E**). This result shows that *Pou4f2* overexpression was able to induce
374   axonogenesis not only at the transcriptional but also at the cellular level, with GFP⁺ projections
375   fasciculating together with the axons of resident RGCs.
376   Previously our group overexpressed *Klf4* in late RPCs and showed the generation of induced
377   RGCs through the activation of an early RGC-program which included the induction of *Eya2 and*
378   *Atoh7*. However, those neurons were not able to extend axons over long distances. Indeed, we found
379   GFP⁺ projections which reached only the initial segment of the optic nerve, failing to reach the optic
380   chiasm or brain regions (Rocha-Martins et al., 2019).
381   Image analysis of the rat visual pathway in longitudinal sections 30 days after *Pou4f2*
382   overexpression detected GFP⁺ projections along the entire optic nerve and crossing the optic chiasm
383   (both ipsilateral and contralateral) (**Figure 6A**).
384   Further, to test whether these projections reached brain regions, we analyzed mouse brain
385   sagittal sections 30 days after *Pou4f2* overexpression. We detected GFP⁺ projections in the superior
386   colliculus, branchium of the superior colliculus, optic tract, and geniculate nucleus (**Figure 6B**). All of
387   these regions are known RGC targets in mice (Martersteck et al., 2017) and we did not see any off-
388   target projections.
389   In conclusion, our study demonstrates that *Pou4f2* overexpression in late RPCs induces the
390   generation of RGC-like cells (RBPMS⁺) located at the GCL and INL, which extend axons toward the
391   optic nerve head, exit the eye, navigate throughout the optic pathway, and reach multiple RGC
392   targets. Additionally, our findings confirm the critical role of POU4F2 in axonogenesis, supported by
393   the identification of POU4F2-direct targets, gene ontology and morphological analyses (**Figure 7**).
394   Since *Pou4f2* overexpression induces genes classified in biological processes related to
395   axonogenesis, we cannot rule out the possibility that in addition to RGC-like cells, other cell types,
396   not expressing RBPMS may have acquired the ability to project axons. This would explain why we

397   identified a high density of projections but a small number of RBPMS⁺GFP⁺ cells, and why in some
398   cases we detect projections at the outer plexiform layer (OPL) (**Figure 1B**) and in the middle of the
399   inner nuclear layer (INL) in transversal sections of the retina. Indeed, some cells from cluster 2 overlap
400   with the RGC cluster (**Figure 4C**) suggesting that they acquired this identity despite maintaining *Sox9*
401   expression, traditionally known as a Müller glia (MG) marker (**Figure S1 E**). Moreover, given that SOX9
402   is expressed by both MG and late RPCs (Poche et al., 2008), we were unable to ascertain whether the
403   expression of *Sox9* in cluster 2, is attributable to an increase in the number of MG or a persistence of
404   undifferentiated RPCs following *Pou4f2* overexpression. Furthermore, comparative analysis revealed
405   that cells from cluster 2 were near the cluster of late RPC which could indicate a transitional stage
406   without a specific mature cell type identity caused by *Pou4f2* overexpression (**Figure 4B-D**). These
407   data suggest that *Pou4f2* overwrites an axonogenesis program in a subset of neurons allowing them
408   to efficiently extend axons up to the brain.
409   Our findings partially contrast with a previous study in which *Pou4f2* was overexpressed in
410   late RPCs. In that study, the authors reported the generation of various cell types, including amacrine
411   cells (GABA⁺, GLYT1⁺, PAX6⁺, CALBINDIN⁺), bipolar cells (CHX10⁺), rod photoreceptors (RECOVERIN⁺),
412   Müller glia (GS⁺) and some unidentified cells, in addition to the generation of RGCs (BRN3a⁺).
413   However, they did not highlight any RGC morphological features in the newly generated cells such as
414   the ability to extend projections up to the brain (Qiu et al., 2008). Regarding the differences between
415   the two studies, the authors did not describe the promoter that was used and employed a different
416   strategy for gene delivery (electroporation *vs.* lentivirus). Different levels of induced *Pou4f2*
417   expression in late RPCs may have contributed to the divergent outcomes observed in the two studies.
418   It is usually expected that in order to regenerate RGCs, certain characteristics need to be
419   achieved, which are: i) specific transcriptional profile; ii) electrophysiological properties; iii)
420   intraretinal connectivity; and iv) ability to project axons to RGC-targets in the brain (Soucy et al.,
421   2023).
422   In this study, we demonstrated that *Pou4f2* overexpression alone is sufficient to efficiently
423   induce at least one critical property of retinal ganglion cells (RGCs): the ability to extend long-distance
424   axon projections. The RGC-like cells also exhibited transcriptional similarities with RGCs characterized
425   previously (Clark et al., 2019). Importantly, as mentioned before, POU4F2 was able to induce these
426   critical RGC features in an efficient manner, enabling projections to reach brain targets, even if the
427   cells did not possess a complete RGC transcriptional profile. Whether these induced neurons function
428   efficiently as RGCs, receiving and transmitting messages to the brain, remains to be fully elucidated.
429   Nonetheless, the generation of axons suggests a potential avenue for restoring vision through
430   communication between the retinal tissue and the brain.
431

References

Amini, R., Rocha-Martins, M., & Norden, C. (2017). Neuronal Migration and Lamination in the Vertebrate Retina. *Front Neurosci* 11**,** 742. doi: 10.3389/fnins.2017.00742.

Bassett, E.A., & Wallace, V.A. (2012). Cell fate determination in the vertebrate retina. *Trends in neurosciences* 35(9)**,** 565-573.

Becht, E., McInnes, L., Healy, J., Dutertre, C.-A., Kwok, I.W.H., Ng, L.G., et al. (2019). Dimensionality reduction for visualizing single-cell data using UMAP. *Nature Biotechnology* 37(1)**,** 38-44. doi: 10.1038/nbt.4314.

Blackshaw, S., Harpavat, S., Trimarchi, J., Cai, L., Huang, H., Kuo, W.P., et al. (2004). Genomic analysis of mouse retinal development. *PLoS biology* 2(9)**,** e247.

Centanin, L., & Wittbrodt, J. (2014). Retinal neurogenesis. *Development* 141(2)**,** 241-244. doi: 10.1242/dev.083642.

Chao, J.R., Lamba, D.A., Klesert, T.R., Torre, A., Hoshino, A., Taylor, R.J., et al. (2017). Transplantation of Human Embryonic Stem Cell-Derived Retinal Cells into the Subretinal Space of a Non-Human Primate. *Transl Vis Sci Technol* 6(3)**,** 4. doi: 10.1167/tvst.6.3.4.

Chow, R.L., and, & Lang, R.A. (2001). EARLY EYE DEVELOPMENT IN VERTEBRATES. *Annu. Rev. Cell Dev. Biol.* 17**,** 255–296.

Clark, B.S., Stein-O'Brien, G.L., Shiau, F., Cannon, G.H., Davis-Marcisak, E., Sherman, T., et al. (2019). Single-Cell RNA-Seq Analysis of Retinal Development Identifies NFI Factors as Regulating Mitotic Exit and Late-Born Cell Specification. *Neuron* 102(6)**,** 1111-1126.e1115. doi: https://doi.org/10.1016/j.neuron.2019.04.010.

Conway, C.D., Price, D.J., Pratt, T., & Mason, J.O. (2011). Analysis of axon guidance defects at the optic chiasm in heparan sulphate sulphotransferase compound mutant mice. *J Anat* 219(6)**,** 734-742. doi: 10.1111/j.1469-7580.2011.01432.x.

Danesh-Meyer, H.V., & Levin, L.A. (2015). Glaucoma as a neurodegenerative disease. *J Neuroophthalmol* 35 Suppl 1**,** S22-28. doi: 10.1097/WNO.0000000000000293.

de Melo, J., Du, G., Fonseca, M., Gillespie, L.A., Turk, W.J., Rubenstein, J.L., et al. (2005). Dlx1 and Dlx2 function is necessary for terminal differentiation and survival of late-born retinal ganglion cells in the developing mouse retina. *Development* 132(2)**,** 311-322. doi: 10.1242/dev.01560.

Dowling, J.E. (1987). *The retina: an approchable part of the brain.* Cambridge and London: The Belknap Press of Harvard University Press.

Dvoriantchikova, G., Seemungal, R.J., & Ivanov, D. (2019). Development and epigenetic plasticity of murine Muller glia. *Biochim Biophys Acta Mol Cell Res* 1866(10)**,** 1584-1594. doi: 10.1016/j.bbamcr.2019.06.019.

Erkman, L., McEvilly, R.J., Luo, L., Ryan, A.K., Hooshmand, F., O'connell, S.M., et al. (1996). Role of transcription factors a Brn-3.1 and Brn-3.2 in auditory and visual system development. *Nature* 381(6583)**,** 603-606.

Erkman, L., Yates, P.A., McLaughlin, T., McEvilly, R.J., Whisenhunt, T., O'Connell, S.M., et al. (2000). A POU domain transcription factor–dependent program regulates axon pathfinding in the vertebrate visual system. *Neuron* 28(3)**,** 779-792.

Fechtner, R.D., & Weinreb, R.N. (1994). Mechanisms of optic nerve damage in primary open angle glaucoma. *Survey of ophthalmology* 39(1)**,** 23-42.

Feng, L., Eisenstat, D., Chiba, S., Ishizaki, Y., Gan, L., & Shibasaki, K. (2011). Brn-3b inhibits generation of amacrine cells by binding to and negatively regulating DLX1/2 in developing retina. *Neuroscience* 195**,** 9-20.

Finlay, B.L., and, & Sengelaub, D.R. (1989). *Development of the Vertebrate Retina.* Plenum Press • New York and London.

480   Gan, L., Wang, S.W., Huang, Z., & Klein, W.H. (1999). POU domain factor Brn-3b is essential for
481   retinal ganglion cell differentiation and survival but not for initial cell fate specification.
482   *Developmental biology* 210(2)**,** 469-480.

483   Gan, L., Xiang, M., Zhou, L., Wagner, D.S., Klein, W.H., & Nathans, J. (1996). POU domain factor Brn-
484   3b is required for the development of a large set of retinal ganglion cells. *Proceedings of the
485   National Academy of Sciences* 93(9)**,** 3920-3925.

486   Gao, Z., Mao, C.A., Pan, P., Mu, X., & Klein, W.H. (2014). Transcriptome of Atoh7 retinal progenitor
487   cells identifies new Atoh7-dependent regulatory genes for retinal ganglion cell formation.
488   *Developmental neurobiology* 74(11)**,** 1123-1140.

489   Ge, Y., Chen, X., Nan, N., Bard, J., Wu, F., Yergeau, D., et al. (2023). Key transcription factors influence
490   the epigenetic landscape to regulate retinal cell differentiation. *Nucleic Acids Research*
491   51(5)**,** 2151-2176.

492   Gossman, C.A., Christie, J., Webster, M.K., Linn, D.M., & Linn, C.L. (2016). Neuroprotective Strategies
493   in Glaucoma. *Curr Pharm Des* 22(14)**,** 2178-2192. doi:
494   10.2174/1381612822666160128144747.

495   Gupta, N., & Yucel, Y.H. (2007). Glaucoma as a neurodegenerative disease. *Curr Opin Ophthalmol*
496   18(2)**,** 110-114. doi: 10.1097/ICU.0b013e3280895aea.

497   Halpern, D.L., & Grosskreutz, C.L. (2002). Glaucomatous optic neuropathy: mechanisms of disease.
498   *Ophthalmology clinics of North America* 15(1)**,** 61-68. doi: 10.1016/s0896-1549(01)00012-
499   8.

500   Heavner, W., & Pevny, L. (2012). Eye development and retinogenesis. *Cold Spring Harb Perspect Biol*
501   4(12). doi: 10.1101/cshperspect.a008391.

502   HÖRNBERG, H., WOLLERTON-VAN HORCK, F., MAURUS, D., ZWART, M., SVOBODA, H., HARRIS, W.A.,
503   et al. (2013). RNA-binding protein Hermes/RBPMS inversely affects synapse density and
504   axon arbor formation in retinal ganglion cells in vivo. *Journal of Neuroscience* 33(25)**,** 10384-
505   10395.

506   Hu, M., and, & Stephen S. Easter, J. (1999). Retinal Neurogenesis: The Formation of the Initial Central
507   Patch of Postmitotic Cells. *Developmental Biology* 207**,** 309–321.

508   Jin, K., & Xiang, M. (2011). Ebf1 deficiency causes increase of Müller cells in the retina and abnormal
509   topographic projection at the optic chiasm. *Biochemical and Biophysical Research
510   Communications* 414(3)**,** 539-544. doi: https://doi.org/10.1016/j.bbrc.2011.09.108.

511   Justin Brodie-Kommit, Brian S. Clark, Qing Shi, Fion Shiau, Dong Won Kim, Jennifer Langel, et al.
512   (2021). Atoh7-independent specification of retinal ganglion cell identity. *SCIENCE
513   ADVANCES* 7(eabe4983). doi: 10.1126/sciadv.abe4983.

514   Killer, H., & Pircher, A. (2018). Normal tension glaucoma: review of current understanding and
515   mechanisms of the pathogenesis. *Eye* 32(5)**,** 924-930.

516   Kruger, K., Tam, A.S., Lu, C., & Sretavan, D.W. (1998). Retinal ganglion cell axon progression from
517   the optic chiasm to initiate optic tract development requires cell autonomous function of
518   GAP-43. *J Neurosci* 18(15)**,** 5692-5705. doi: 10.1523/jneurosci.18-15-05692.1998.

519   Le, T.T., Wroblewski, E., Patel, S., Riesenberg, A.N., & Brown, N.L. (2006). Math5 is required for both
520   early retinal neuron differentiation and cell cycle progression. *Developmental biology*
521   295(2)**,** 764-778.

522   Li, R., Wu, F., Ruonala, R., Sapkota, D., Hu, Z., & Mu, X. (2014). Isl1 and Pou4f2 form a complex to
523   regulate target genes in developing retinal ganglion cells. *PLoS One* 9(3)**,** e92105. doi:
524   10.1371/journal.pone.0092105.

525   Liu, W., Khare, S.L., Liang, X., Peters, M.A., Liu, X., Cepko, C.L., et al. (2000). All Brn3genes can
526   promote retinal ganglion cell differentiation in the chick. *Development* 127**,** 3237-3247.

527   Liu, W., Mo, Z., & Xiang, M. (2001). The Ath5 proneural genes function upstream of Brn3 POU
528   domain transcription factor genes to promote retinal ganglion cell development.
529   *Proceedings of the National Academy of Sciences* 98(4)**,** 1649-1654.
530   Livesey, F., & Cepko, C. (2001). Vertebrate neural cell-fate determination: lessons from the retina.
531   *Nature Reviews Neuroscience* 2(2)**,** 109.
532   Luo, Z., & Chang, K.-C. (2023). Cell replacement with stem cell-derived retinal ganglion cells from
533   different protocols. *Neural Regeneration Research*.
534   Macosko, E.Z., Basu, A., Satija, R., Nemesh, J., Shekhar, K., Goldman, M., et al. (2015). Highly Parallel
535   Genome-wide Expression Profiling of Individual Cells Using Nanoliter Droplets. *Cell* 161(5)**,**
536   1202-1214. doi: 10.1016/j.cell.2015.05.002.
537   Mao, C.-A., Kiyama, T., Pan, P., Furuta, Y., Hadjantonakis, A.-K., & Klein, W.H. (2008). Eomesodermin,
538   a target gene of Pou4f2, is required for retinal ganglion cell and optic nerve development in
539   the mouse. *Development* 135(2)**,** 271-280. doi: 10.1242/dev.009688.
540   Martersteck, E.M., Hirokawa, K.E., Evarts, M., Bernard, A., Duan, X., Li, Y., et al. (2017). Diverse
541   Central Projection Patterns of Retinal Ganglion Cells. *Cell Rep* 18(8)**,** 2058-2072. doi:
542   10.1016/j.celrep.2017.01.075.
543   Matsuda, T., & Cepko, C.L. (2004). Electroporation and RNA interference in the rodent retina in vivo
544   and in vitro. *Proc Natl Acad Sci U S A* 101(1)**,** 16-22. doi: 10.1073/pnas.2235688100

545   2235688100 [pii].
546   Matsuda, T., & Cepko, C.L. (2007). Controlled expression of transgenes introduced by in vivo
547   electroporation. *Proc Natl Acad Sci U S A* 104(3)**,** 1027-1032. doi:
548   10.1073/pnas.0610155104.
549   Maurer, K.A., Kowalchuk, A., Shoja-Taheri, F., & Brown, N.L. (2018). Integral bHLH factor regulation
550   of cell cycle exit and RGC differentiation. *Developmental Dynamics* 247(8)**,** 965-975. doi:
551   10.1002/dvdy.24638.
552   McNeill, E.M., Roos, K.P., Moechars, D., & Clagett-Dame, M. (2010). Nav2 is necessary for cranial
553   nerve development and blood pressure regulation. *Neural development* 5**,** 1-14.
554   Miesfeld, J.B., Glaser, T., & Brown, N.L. (2018). The dynamics of native Atoh7 protein expression
555   during mouse retinal histogenesis, revealed with a new antibody. *Gene Expr Patterns* 27**,**
556   114-121. doi: 10.1016/j.gep.2017.11.006.
557   Mu, X., Fu, X., Sun, H., Beremand, P.D., Thomas, T.L., & Klein, W.H. (2005). A gene network
558   downstream of transcription factor Math5 regulates retinal progenitor cell competence and
559   ganglion cell fate. *Developmental Biology* 280(2)**,** 467-481.
560   Nakaya, N., Lee, H.S., Takada, Y., Tzchori, I., & Tomarev, S.I. (2008). Zebrafish olfactomedin 1
561   regulates retinal axon elongation in vivo and is a modulator of Wnt signaling pathway. *J
562   Neurosci* 28(31)**,** 7900-7910. doi: 10.1523/jneurosci.0617-08.2008.
563   Nakaya, N., Sultana, A., Lee, H.S., & Tomarev, S.I. (2012). Olfactomedin 1 interacts with the Nogo A
564   receptor complex to regulate axon growth. *J Biol Chem* 287(44)**,** 37171-37184. doi:
565   10.1074/jbc.M112.389916.
566   Nawabi, H., Belin, S., Cartoni, R., Williams, Philip R., Wang, C., Latremolière, A., et al. (2015).
567   Doublecortin-Like Kinases Promote Neuronal Survival and Induce Growth Cone Reformation
568   via Distinct Mechanisms. *Neuron* 88(4)**,** 704-719. doi:
569   https://doi.org/10.1016/j.neuron.2015.10.005.
570   Oliveira-Valenca, V.M., Bosco, A., Vetter, M.L., & Silveira, M.S. (2020). On the Generation and
571   Regeneration of Retinal Ganglion Cells. *Front Cell Dev Biol* 8**,** 581136. doi:
572   10.3389/fcell.2020.581136.

573 Ooto, S., Akagi, T., Kageyama, R., Akita, J., Mandai, M., Honda, Y., et al. (2004). Potential for neural
574   regeneration after neurotoxic injury in the adult mammalian retina. *Proceedings of the*
575   *National Academy of Sciences of the United States of America* 101(37)**,** 13654-13659.
576 Pan, L., Deng, M., Xie, X., & Gan, L. (2008). ISL1 and BRN3B co-regulate the differentiation of murine
577   retinal ganglion cells. *Development* 135(11)**,** 1981-1990. doi: 10.1242/dev.010751.
578 Poche, R.A., Furuta, Y., Chaboissier, M.C., Schedl, A., & Behringer, R.R. (2008). Sox9 is expressed in
579   mouse multipotent retinal progenitor cells and functions in Muller glial cell development. *J*
580   *Comp Neurol* 510(3)**,** 237-250. doi: 10.1002/cne.21746.
581 Qiu, F., Jiang, H., & Xiang, M. (2008). A comprehensive negative regulatory program controlled by
582   Brn3b to ensure ganglion cell specification from multipotential retinal precursors. *J Neurosci*
583   28(13)**,** 3392-3403. doi: 10.1523/JNEUROSCI.0043-08.2008.
584 Quigley, H.A. (1995). Ganglion cell death in glaucoma: pathology recapitulates ontogeny. *Australian*
585   *and New Zealand journal of ophthalmology* 23(2)**,** 85-91.
586 Quigley, H.A. (1999). Neuronal death in glaucoma. *Progress in retinal and eye research* 18(1)**,** 39-57.
587 Rapaport, D.H., Wong, L.L., Wood, E.D., Yasumura, D., & LaVail, M.M. (2004). Timing and topography
588   of cell genesis in the rat retina. *J Comp Neurol* 474(2)**,** 304-324. doi: 10.1002/cne.20134.
589 Rasheed, V.A., Sreekanth, S., Dhanesh, S.B., Divya, M.S., Divya, T.S., Akhila, P.K., et al. (2014).
590   Developmental wave of Brn3b expression leading to RGC fate specification is synergistically
591   maintained by miR-23a and miR-374. *Dev Neurobiol* 74(12)**,** 1155-1171. doi:
592   10.1002/dneu.22191.
593 Reh, T.A., Redshaw, J.D., & Bisby, M.A. (1987). Axons of the pyramidal tract do not increase their
594   transport of growth-associated proteins after axotomy. *Brain Res* 388(1)**,** 1-6.
595 Rheaume, B.A., Jereen, A., Bolisetty, M., Sajid, M.S., Yang, Y., Renna, K., et al. (2018). Single cell
596   transcriptome profiling of retinal ganglion cells identifies cellular subtypes. *Nat Commun*
597   9(1)**,** 2759. doi: 10.1038/s41467-018-05134-3.
598 Rocha-Martins, M.c., de Toledo, B.C., Santos-França, P.L., Oliveira-Valença, V.M., Vieira-Vieira, C.H.,
599   Matos-Rodrigues, G.E., et al. (2019). *De novo* genesis of retinal ganglion cells by targeted
600   expression of *Klf4 in vivo*. *Development* 146(16)**,** dev176586. doi: 10.1242/dev.176586.
601 Rodriguez, A.R., Müller, S., Pérez, L., & Brecha, N.C. (2014). The RNA binding protein RBPMS is a
602   selective marker of ganglion cells in the mammalian retina. *Journal of Comparative*
603   *Neurology* 522(6)**,** 1411-1443.
604 Roesch, K., Jadhav, A.P., Trimarchi, J.M., Stadler, M.B., Roska, B., Sun, B.B., et al. (2008). The
605   transcriptome of retinal Muller glial cells. *J Comp Neurol* 509(2)**,** 225-238. doi:
606   10.1002/cne.21730.
607 Rousso, David L., Qiao, M., Kagan, Ruth D., Yamagata, M., Palmiter, Richard D., & Sanes, Joshua R.
608   (2016). Two Pairs of ON and OFF Retinal Ganglion Cells Are Defined by Intersectional
609   Patterns of Transcription Factor Expression. *Cell Reports* 15(9)**,** 1930-1944. doi:
610   https://doi.org/10.1016/j.celrep.2016.04.069.
611 Saha, M.S., Servetnick, M., and, & Grainger, R.M. (1992). Vertebrate eye development. *Current*
612   *Opinion in Genetics and Development* 2**,** 582-588.
613 Sato, C., Iwai-Takekoshi, L., Ichikawa, Y., & Kawasaki, H. (2017). Cell type-specific expression of FoxP2
614   in the ferret and mouse retina. *Neuroscience Research* 117**,** 1-13. doi:
615   https://doi.org/10.1016/j.neures.2016.11.008.
616 Sharma, T.P., Ho, K., Bodi, N., & Hameed, S.S. (2023). Transplantation strategy of human retinal
617   ganglion cells for glaucoma. *Investigative Ophthalmology & Visual Science* 64(8)**,** 3846-3846.
618 Shi, M., Kumar, S.R., Motajo, O., Kretschmer, F., Mu, X., & Badea, T.C. (2013). Genetic interactions
619   between Brn3 transcription factors in retinal ganglion cell type specification. *PloS one* 8(10)**,**
620   e76347.

621 Soucy, J.R., Aguzzi, E.A., Cho, J., Gilhooley, M.J., Keuthan, C., Luo, Z., et al. (2023). Retinal ganglion
622   cell repopulation for vision restoration in optic neuropathy: a roadmap from the RReSTORe
623   Consortium. *Molecular Neurodegeneration* 18(1)**,** 64. doi: 10.1186/s13024-023-00655-y.
624 Tanaka, T., Yokoi, T., Tamalu, F., Watanabe, S.-I., Nishina, S., & Azuma, N. (2016). Generation of
625   retinal ganglion cells with functional axons from mouse embryonic stem cells and induced
626   pluripotent stem cells. *Investigative ophthalmology & visual science* 57(7)**,** 3348-3359.
627 Tham, Y.-C., Li, X., Wong, T.Y., Quigley, H.A., Aung, T., & Cheng, C.-Y. (2014). Global prevalence of
628   glaucoma and projections of glaucoma burden through 2040: a systematic review and meta-
629   analysis. *Ophthalmology* 121(11)**,** 2081-2090.
630 Todd, L., Jenkins, W., Finkbeiner, C., Hooper, M.J., Donaldson, P.C., Pavlou, M., et al. (2022).
631   Reprogramming Muller glia to regenerate ganglion-like cells in adult mouse retina with
632   developmental transcription factors. *Sci Adv* 8(47)**,** eabq7219. doi: 10.1126/sciadv.abq7219.
633 Tribble, J.R., Hui, F., Quintero, H., El Hajji, S., Bell, K., Di Polo, A., et al. (2023). Neuroprotection in
634   glaucoma: Mechanisms beyond intraocular pressure lowering. *Molecular Aspects of*
635   *Medicine* 92**,** 101193.
636 Wu, F., Bard, J.E., Kann, J., Yergeau, D., Sapkota, D., Ge, Y., et al. (2021). Single cell transcriptomics
637   reveals lineage trajectory of retinal ganglion cells in wild-type and Atoh7-null retinas. *Nature*
638   *communications* 12(1)**,** 1-20.
639 Wu, F., Kaczynski, T.J., Sethuramanujam, S., Li, R., Jain, V., Slaughter, M., et al. (2015). Two
640   transcription factors, Pou4f2 and Isl1, are sufficient to specify the retinal ganglion cell fate.
641   *Proc Natl Acad Sci U S A* 112(13)**,** E1559-1568. doi: 10.1073/pnas.1421535112.
642 Xiang, M. (1998). Requirement for Brn-3b in early differentiation of postmitotic retinal ganglion cell
643   precursors. *Developmental biology* 197(2)**,** 155-169.
644 Xiang, M., Zhoui, L., Macke, J.P., Yoshioka, T., Hendry, S.H.C., Eddy, R.L., et al. (1996). The Brn-3
645   Family of POU-Domain Factors: Primary Structure, Binding Specificity, and Expression in
646   subset of Retinal Ganglion Cells and Somatosensory Neurons. *Journal of Neuroscience* 15**,**
647   4762-4785.
648 Yang, Z., Ding, K., Pan, L., Deng, M., & Gan, L. (2003). Math5 determines the competence state of
649   retinal ganglion cell progenitors. *Developmental biology* 264(1)**,** 240-254.
650 Yao, J., Sun, X., Wang, Y., Xu, G., & Qian, J. (2007). Math5 promotes retinal ganglion cell expression
651   patterns in retinal progenitor cells. *Molecular Vision* 13**,** 1066.
652 Young, R.W. (1985). Cell differentiation in the retina of the mouse. *The Anatomical Record* 212(2)**,**
653   199-205.
654 Young, T.R., Black, D., Mansuri, H., Oohashi, T., Zhou, X.H., Sawatari, A., et al. (2023). Ten-m4 plays
655   a unique role in the establishment of binocular visual circuits. *Dev Neurobiol* 83(3-4)**,** 104-
656   124. doi: 10.1002/dneu.22912.
657 Zechner, C., Nerli, E., & Norden, C. (2020). Stochasticity and determinism in cell fate decisions.
658   *Development* 147(14). doi: 10.1242/dev.181495.
659 Zhang, Q., Zagozewski, J., Cheng, S., Dixit, R., Zhang, S., de Melo, J., et al. (2017). Regulation of Brn3b
660   by DLX1 and DLX2 is required for retinal ganglion cell differentiation in the vertebrate retina.
661   *Development* 144(9)**,** 1698-1711.

662

663

664

665

666

Authors Contributions

Conceptualization: M.R.-M, M.S.S. and V.M.O.-V; Methodology: V.M.O-V, J.M.R and M.S.S Validation: V.M.O-V and M.S.S.; image analysis: V.M.O.-V, V.M.F-C and C.H.C.; Bioinformatic analysis: J.M.R.; Investigation: V.M.O-V, V.M.F-C, C.H.C, B.C.d.T, P.L.S.-F, M.R-M., J.M.R. and M.S.S.; Writing – review & editing: V.M.O.-V, J.M.R., M.L.V., A.B., P.L.S.-F, R.A.P.M., M.R.M., R.L. and M.S.S.; Supervision: M.S.S.; Project Funding Administration: M.S.S. Funding acquisition: M.S.S., A.B., M.L.V., R.A.P.M. and R.L.

Declaration of interests

The authors declare no conflict of interests.

Funding

696   Figure legends

697

698   **Figure 1:** *Pou4f2* **promotes the production of RGC-like neurons with complex morphology. (A)**

699   Experimental design. Rats were electroporated *in vivo* on the date of birth (P0) to induce

700   overexpression of GFP (Control) or Pou4f2 and GFP (Pou4f2), followed by analysis after 10 or 30 days

701   (P10 or P30). For EdU labeling of proliferating cells, EdU injections were performed at P0 and P1,

702   followed by eye electroporation at P1 and harvest after 10 days (design in pink). **(B)** Representative

703   images of radial retinal sections of Control and Pou4f2 conditions after 10 days. **(C)** Quantification of

704   the percentage of GFP⁺ cells at each retinal cell layer (2way ANOVA with Sidak's test n=4-5). **(D)**

705   Retinal wholemounts from 30 days after *Pou4f2* electroporation showed GFP⁺RBPMS⁺ cells (yellow

706   arrowhead) located at the GCL (left panel) and INL (right panel). Morphology of some *Pou4f2*-induced

707   neurons is complex with abundant dendrites and an axon. **(E)** Proportion of RBPMS⁺ (RGC marker)

708   and NEUN⁺ (RGC and AC marker) cells in the electroporated population analyzed after 10 days (2way

709   ANOVA with Sidak's test, n=3-4). **(F)** Radial retinal sections showing EdU labelling used to trace late

710   RPCs and their progeny 10 days post electroporation. Some RBPMS⁺GFP⁺ cells generated upon *Pou4f2*

711   overexpression were EdU⁺ (yellow arrowhead), while others were RBPMS⁺GFP⁺EdU⁻ (white

712   arrowhead). **(G)** Proportion of RBPMS⁺GFP⁺EdU⁺ cells among cycling, electroporated cells (GFP⁺EdU⁺)

713   (unpaired t-test, two-tailed, n=3). For all bar plots each dot represents one animal, bars are mean

714   ±SEM and p-values are shown above the bars. EPN – electroporation; ONL – Outer Nuclear Layer;

715   OPL – Outer Plexiform Layer; oINL- Inner nuclear layer, outer region; mINL- Inner nuclear layer,

716   middle region; iINL - Inner nuclear layer, inner region; IPL – Inner Plexiform Layer; GCL – Ganglion Cell

717   Layer; NFL – Nerve Fiber Layer. Scale bar 50µm.

718

719   **Figure 2: scRNA-seq analysis reveals that** *Pou4f2* **overexpression induces several RGC-genes.** Neonate

720   mice were electroporated *in vivo* (P0) with Gfp (Control) or Pou4f2+Gfp (Pou4f2OE), and after 10

721   days, retinas were dissociated, GFP⁺ cells collected by FACS, and analyzed by scRNA-seq. **(A)** UMAP

722   plot colored to distinguish control cells (gray) from Pou4f2OE cells (light blue). **(B)** UMAP graph

723   colored by cluster. **(C)** Split UMAPs showing that the new clusters 1-4 are specific for Pou4f2 OE

724   retinas. **(D)** UMAP graphs showing the expression of four RGC-genes (*Rbpms, Hs6st3, Foxp2 and*

725   *GAP43*). Purple indicates high gene expression levels and gray the absence of gene expression. **(E)**

726   Immunostaining for GAP-43 validates the scRNA-seq result of *Pou4f2* inducing the expression of this

727   gene in some GFP⁺ cells (yellow arrowhead), which is not observed in control condition. **(F)**

728   Intersection between upregulated genes from Pou4f2 OE scRNA-seq (light blue) and previous

729   published CUT&TAG for POU4F2 targets (purple) (Ge et al., 2023).

730

731   **Figure 3: Aberrant projections are detected after** *Pou4f2* **overexpression in the Atoh7KO mice.**

732   Neonate Atoh7KO mice were electroporated *in vivo* (P1) with Gfp (Control; n=2) or Pou4f2+Gfp

733   (POU4F2OE; n=2), and after 10 days, retinas were immunostained for GFP (green). **(A)** Wholemount

734   retinas from each condition (control in the left and Pou4f2OE in the right panel) show electroporated

735   cells (GFP⁺) distributed in the retinal layers: ONL (first line), INL (middle line) and IPL+GCL (third line).

736   GFP+ cells are found in the IPL+GLC (A inset 6; yellow arrowhead indicates the putative axon) while

737   only MG endfeet are detected in Control **(A inset 3, white arrowheads). (B)** After *Pou4f2*

738   overexpression random GFP$^+$ axons (yellow arrowheads) are found in the periphery of the retina. The

739   same is not observed in the control condition. ONL – Outer Nuclear Layer; INL- Inner nuclear layer;

740   IPL – Inner Plexiform Layer; GCL – Ganglion Cell Layer. Scale bar 50μm.

741

742   **Figure 4: RGC-like cells are clustered near endogenous RGCs.** ScRNA-seq dataset from CTR and Pou4f2

743   overexpression conditions were integrated with published data from E11-P14 retinas (Clark et al.,

744   2019). **(A)** UMAP graph showing both datasets integrated. Clusters 1-4 are the new clusters identified

745   after *Pou4f2* overexpression. **(B)** UMAP graph showing cells from the dataset generated in this paper

746   (colored cells), overlapped with Clark et al (2019) dataset (gray). **(C)** Recoloring cells that are closest

747   to the RGC cluster in dark gray reveals that cells from clusters 1-4 are found in this group. **(D)** Plotting

748   of these RGC-like cells in the UMAP generated from our dataset, using the same colors as in **C**, clearly

749   identifies subpopulations in clusters 1 and 2.

750

751   **Figure 5: *Pou4f2* overexpression induces axonogenesis.** Retinas from mice **(A-C)** or rats **(D-E)** were

752   electroporated *in vivo* on the date of birth (P0) for the overexpression of Gfp (Control) or Pou4f2+Gfp

753   (Pou4f2 OE). After 10 and 30 days, tissues were harvested for dissociation for scRNA-seq or

754   immunostaining. **(A)** Gene ontology analysis of scRNA-seq data reveals the *Pou4f2* induced (in red to

755   orange) and downregulated (in blue) processes. **(B)** Volcano plot shows the distribution of

756   differentially regulated genes in scRNA-seq. Genes of phototransduction (blue dots) and axon

757   development (red dots) are highlighted. **(C)** UMAPs show the expression of some axonogenesis

758   regulators (*Olfm1*, *Tubb3*, *Dclk1* and *Tenm4*) in the *Pou4f2*-induced clusters. Purple indicates high

759   gene expression levels and gray the absence of gene expression. Representative images from optic

760   nerve head **(D)** and wholemounted retinas **(E)** show a high density of GFP$^+$ projections in the Pou4f2

761   OE retina. Scale bar 50 μm **(D)** and 100 μm **(E)**. ONH- optic nerve head. GCL – Ganglion Cell Layer, NFL

762   – Nerve Fiber Layer.

763

764   **Figure 6: RGC-like cells project eye-to-brain axons.** Analysis of GFP$^+$ axon extraretinal extension, 30

765   days after electroporation. **(A)** Optic nerve image reconstruction shows GFP$^+$ axons (green, yellow

766   arrowhead) present at the nerve and the chiasm in rats. Insets show high-magnification views at the

767   nerve (1-3) and chiasm (4). White arrowheads indicate non-specific labeling. **(B)** Mouse brain

768   orthogonal images from sagittal brain sections stained for Hoechst, showing GFP$^+$ axons (white) at

769   the optic tract, and reaching the superior colliculus and geniculate nucleus. Scale bar 500μm **(A)** and

770   50μm **(B)**.

771

772   **Figure 7: *Pou4f2* induces neurogenesis and axonogenesis of RGC-like cells in a subset of late RPCs.**

773   Schematic representation of Control and Pou4f2-overexpressed retinas and visual pathway. In

774   control condition, late RPCs generate rod photoreceptors, bipolar cells, Müller glia and some

775   amacrine cells. *Pou4f2* overexpression induced the generation of RGC-like cells and a high density of

776   projections toward the optic nerve head up to RGC projection areas, such as geniculate nucleus (GN)

777   and superior colliculus (SC). OPT – optic tract.

778

779 **Figure S1:** *Pou4f2* **reduces the number of rod photoreceptors**. Rats were electroporated *in vivo* on
780 the date of birth (P0) to overexpress Gfp (Control) or Pou4f2+Gfp (Pou4f2) and analyzed 10 days later.
781 Images of representative radial retina sections immunostained for: **(A)** SOX9 (Müller glia marker,
782 gray); **(B)** CHX10 (Bipolar cells, gray) and **(C)** Rhodopsin (RHO, rod photoreceptors, grey). Cells with
783 Late Marker+GFP+ are indicated with a yellow arrowhead in all conditions. **(D)** Quantification of the
784 proportion of LateMarker+GFP+ cells in the electroporated population (2way ANOVA with Sidak's test
785 n=3-5). Fewer RHO+GFP+ cells were detected in POU4F2 condition. **(E)** Graph shows the proportion
786 of each cell type identified in the scRNA-seq analysis between conditions. EPN – electroporation; ONL
787 – Outer Nuclear Layer; OPL – Outer Plexiform Layer; INL- Inner nuclear layer; IPL – Inner Plexiform
788 Layer; GCL – Ganglion Cell Layer. Scale bar 50μm.
789

790 **Figure S2: Most POU4F2 direct targets are expressed by the new cell clusters generated after** *Pou4f2*
791 **overexpression.** UMAPs of the 33 genes found in the intersection from the upregulated genes from
792 our scRNA-seq and POU4F2 CUT&TAG data from Ge et al. (2023). Purple indicates high-gene
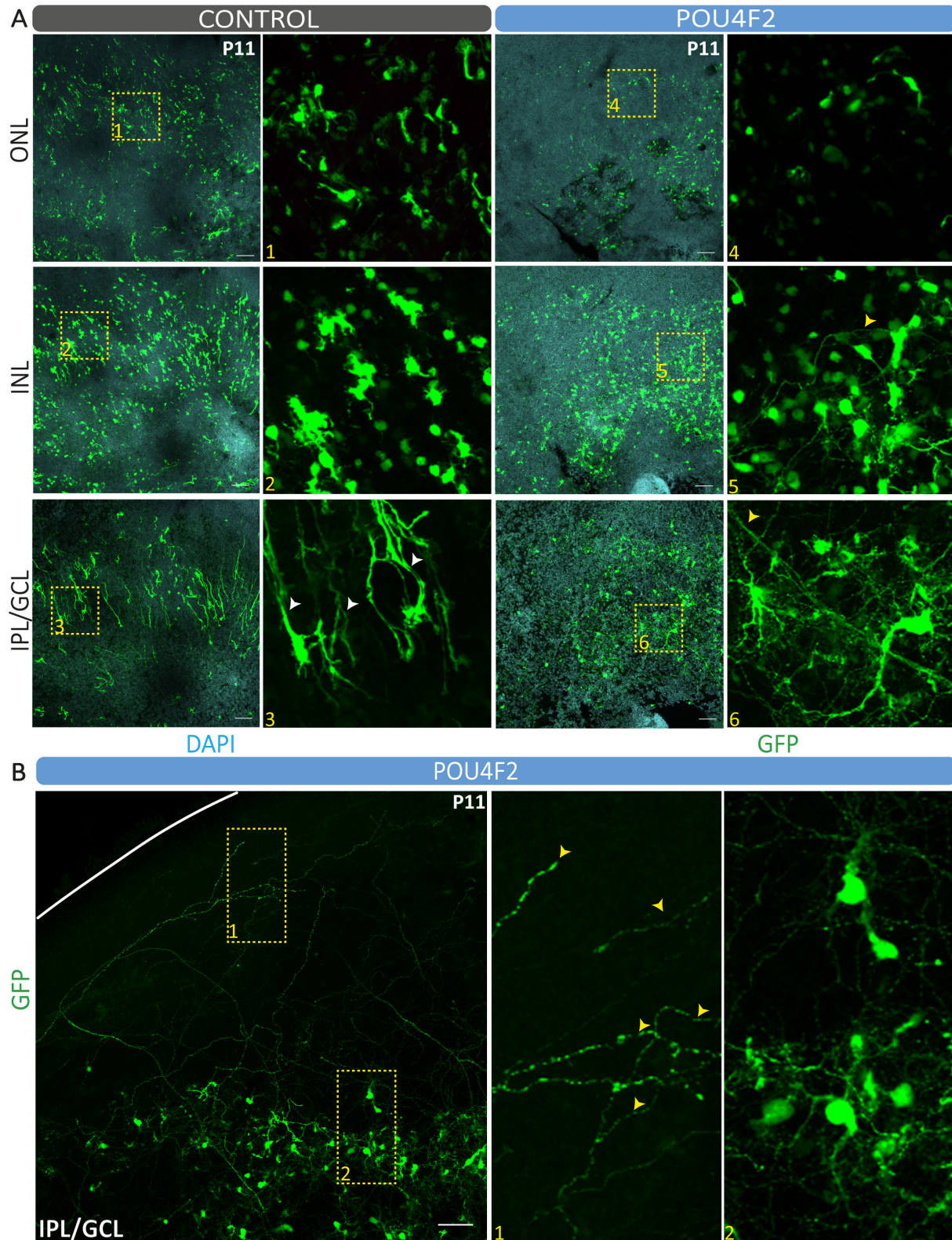793 expression levels and gray the absence of gene expression.
794

Oliveira-Valença *et al*, Figure 1
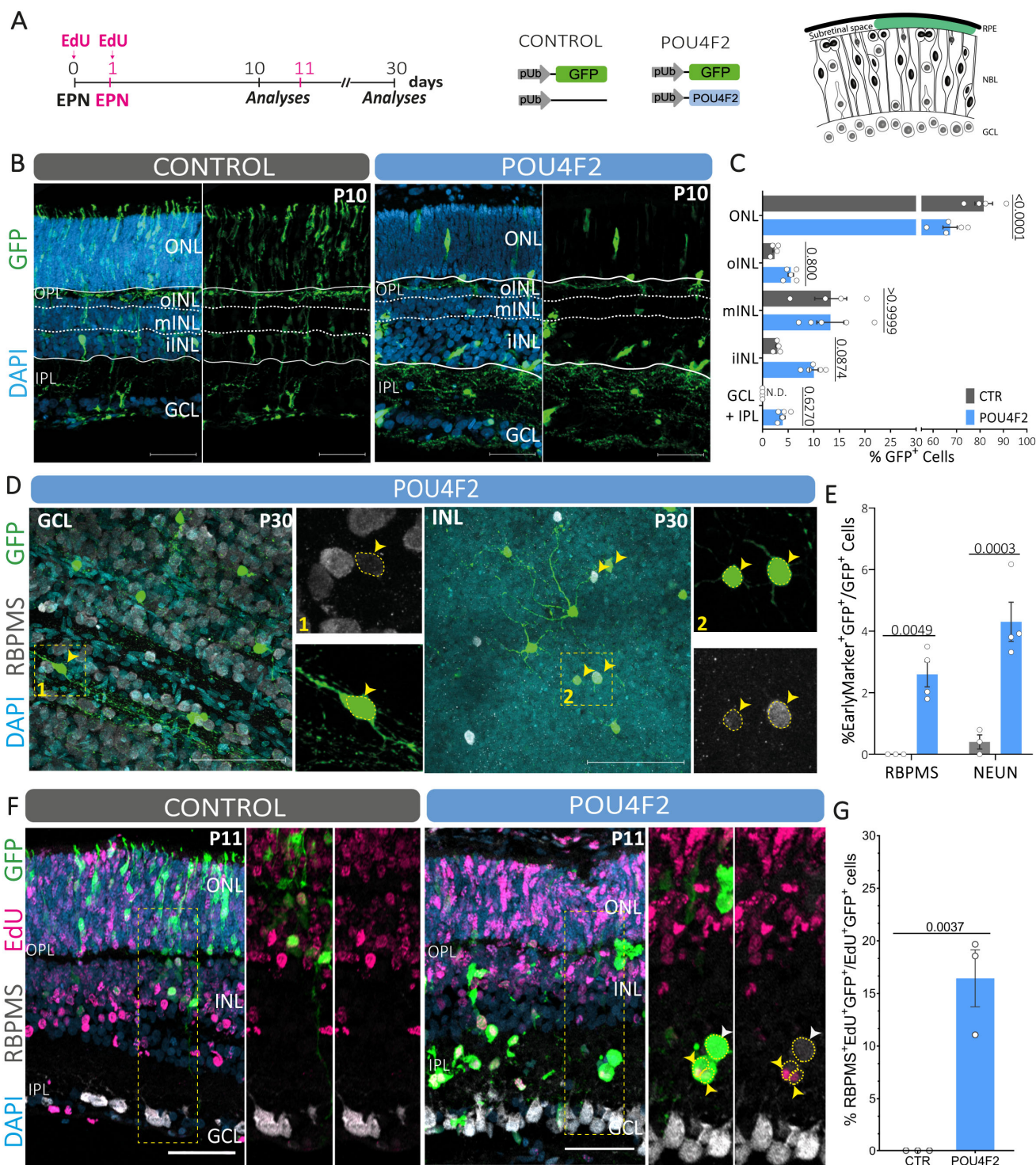
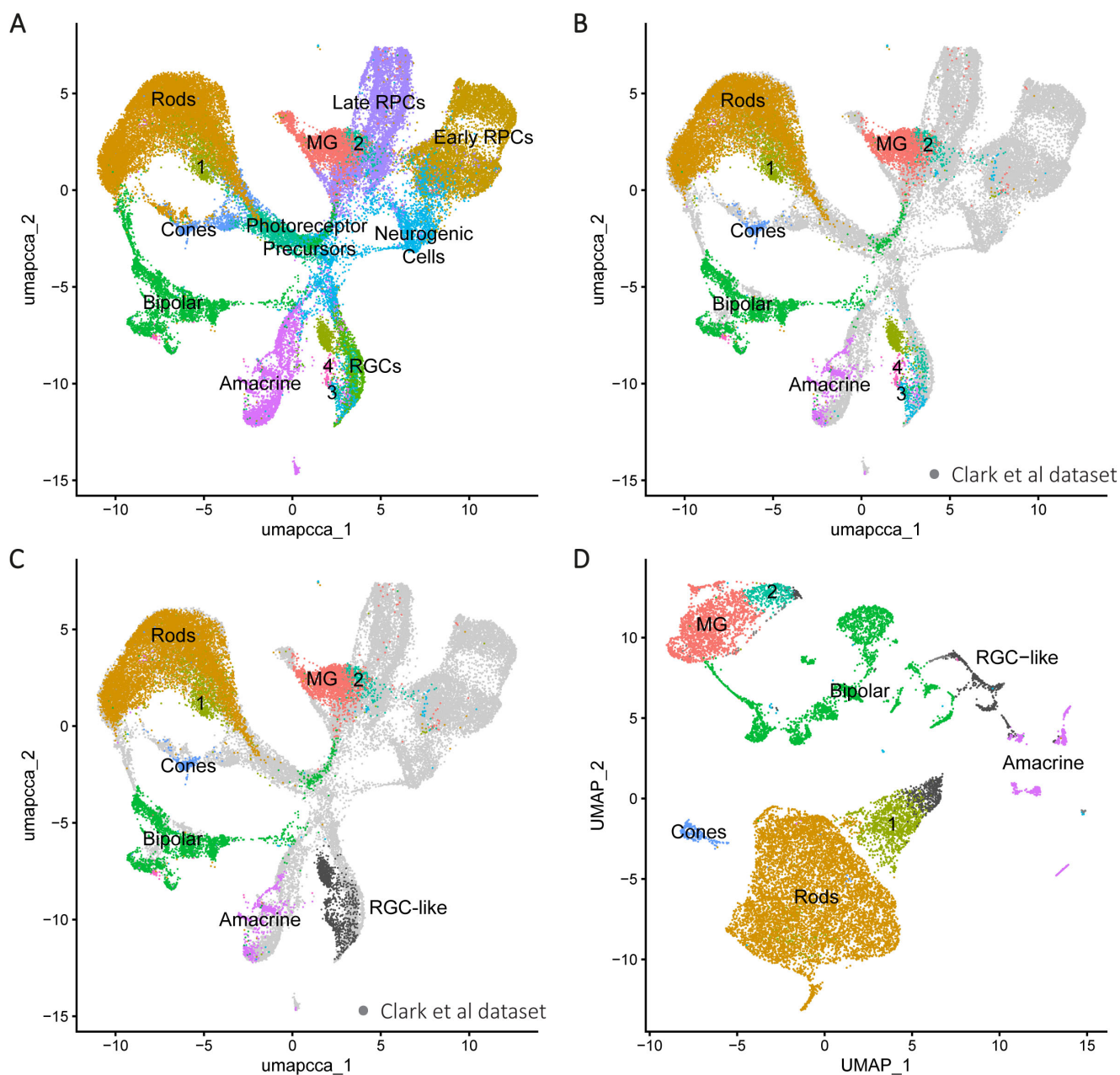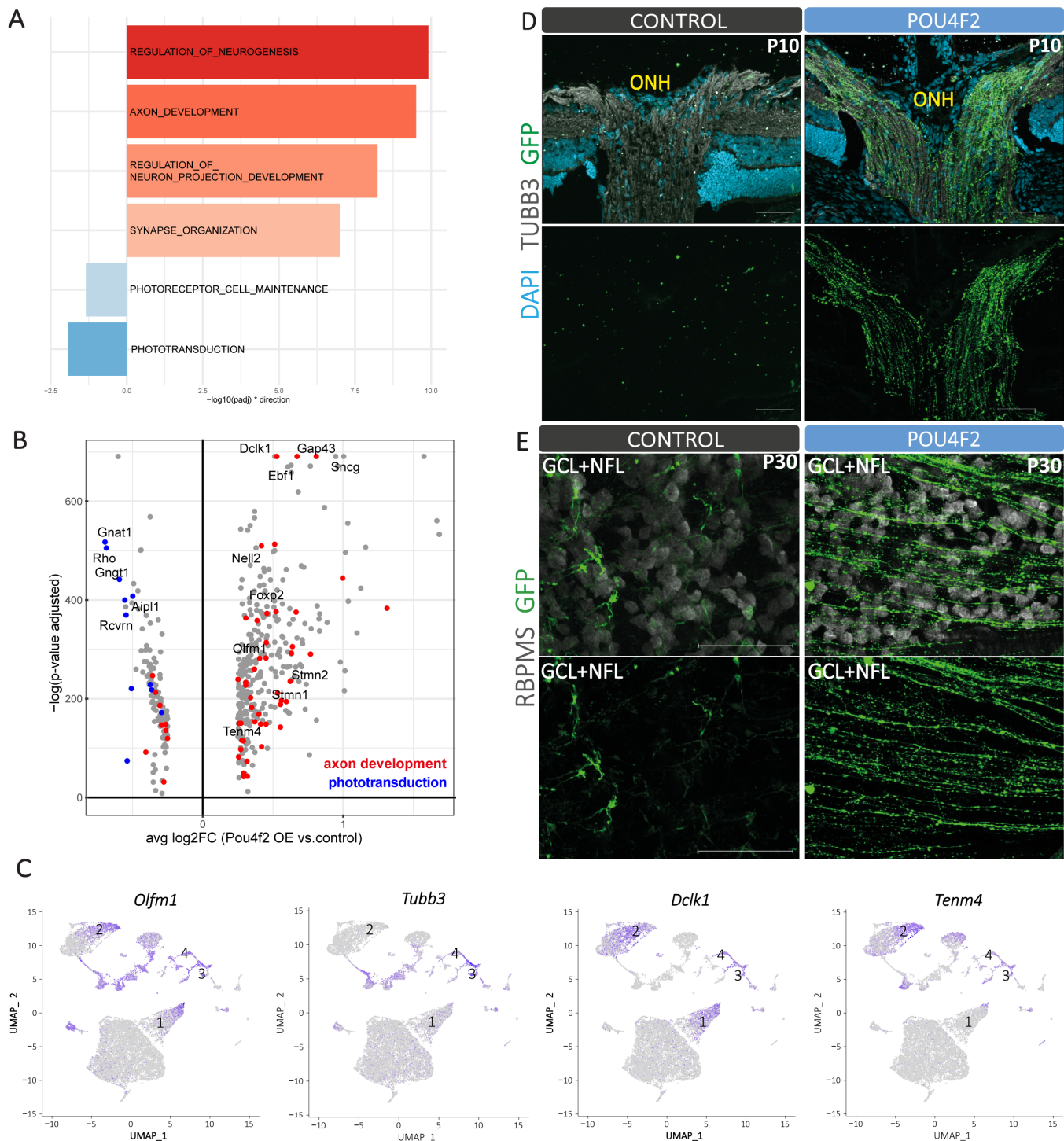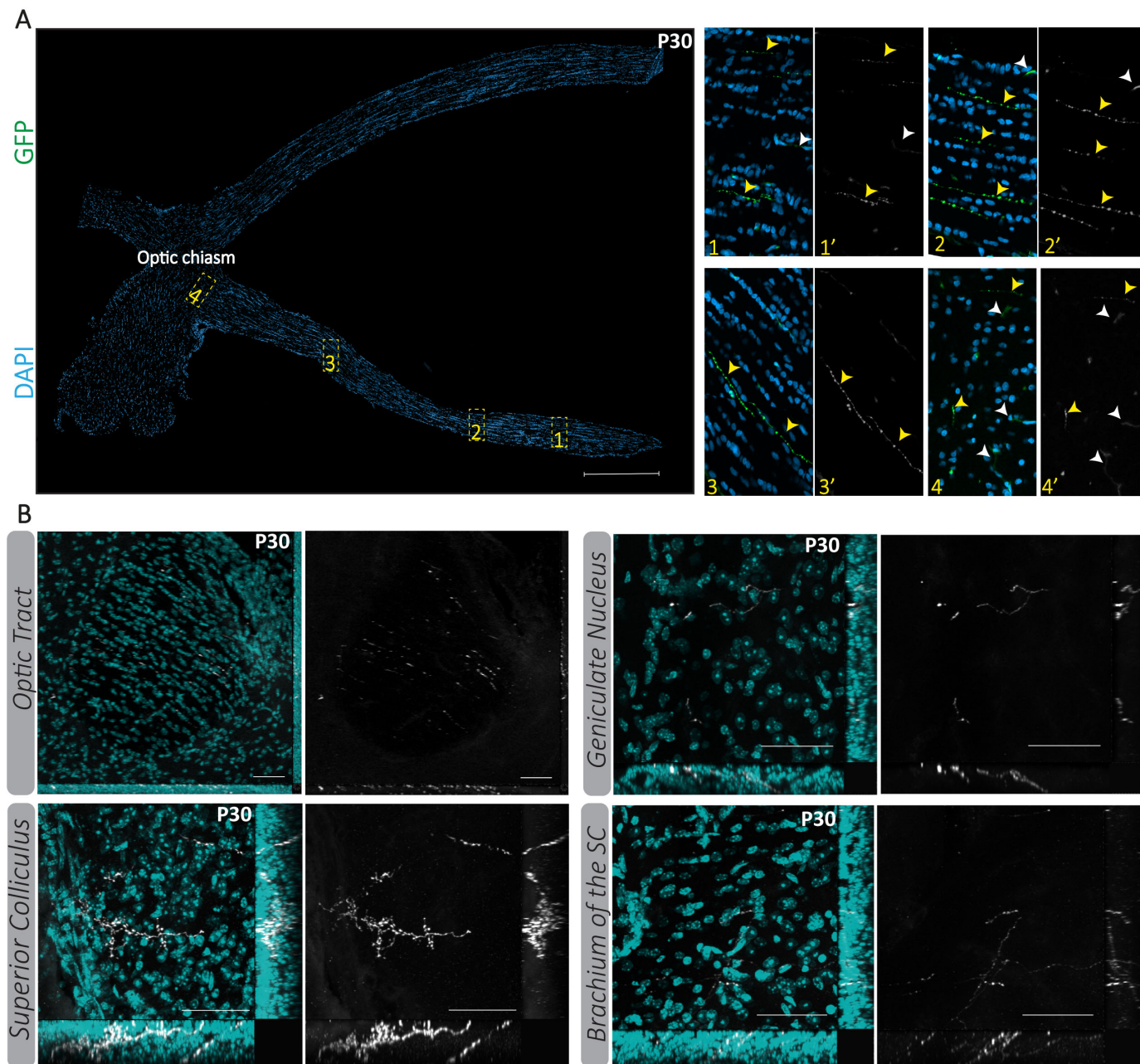Oliveira-Valença *et al*, Figure 2
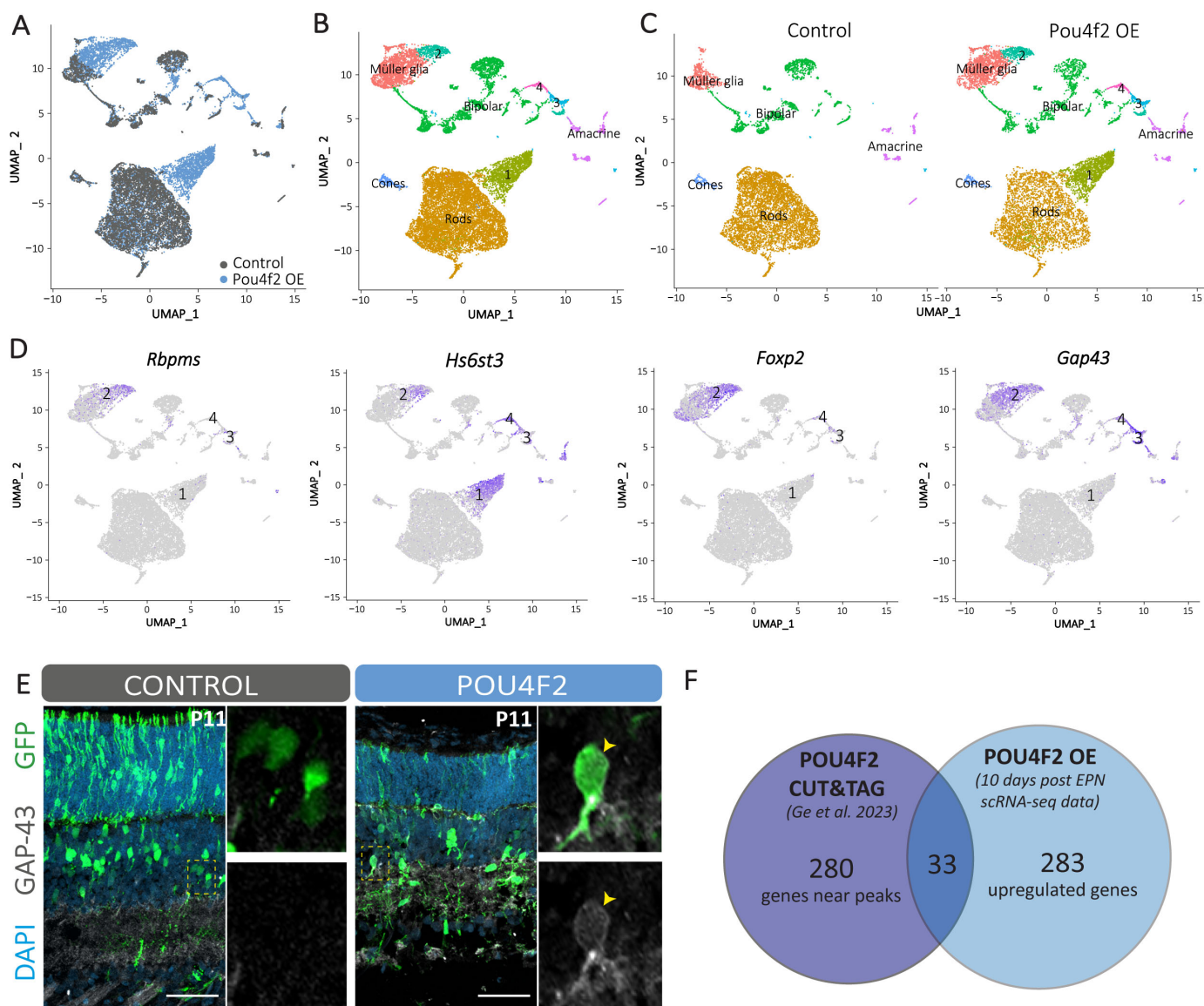
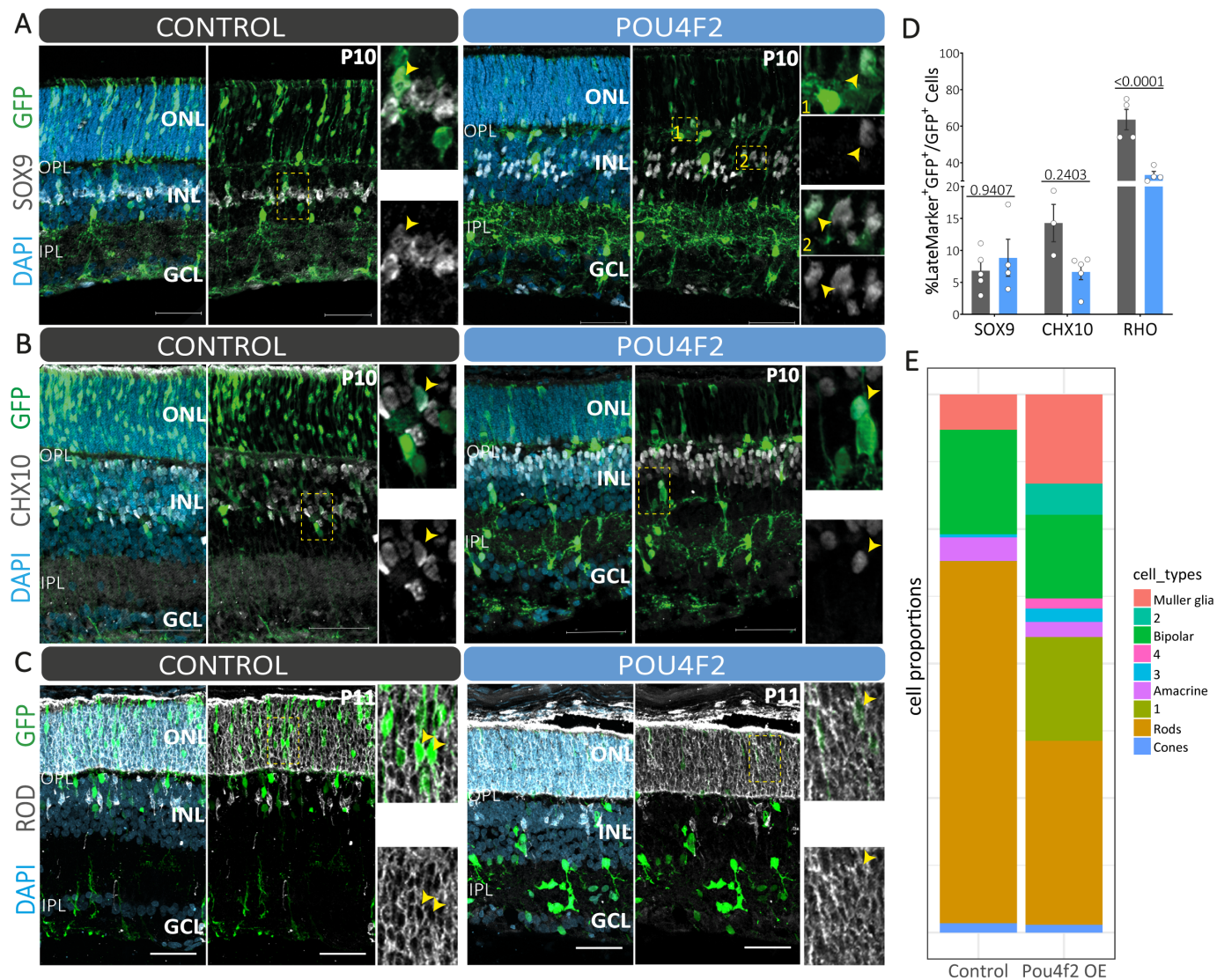Oliveira-Valença *et al*, Figure 3

Oliveira-Valença *et al*, Figure 4

Oliveira-Valença *et al*, Figure 5

Oliveira-Valença *et al*, Figure 6

Oliveira-Valença *et al*, Figure 7

CONTROL

POU4F2 OE

Oliveira-Valença *et al*, Figure S1

Oliveira-Valença *et al*, Figure S2